

Contents lists available at ScienceDirect

Physics Letters B

www.elsevier.com/locate/physletbTwo-proton capture on the ^{68}Se nucleus with a new self-consistent cluster modelD. Hove^{a,*}, E. Garrido^b, A.S. Jensen^a, P. Sarriguren^b, H.O.U. Fynbo^a, D.V. Fedorov^a, N.T. Zinner^a^a Department of Physics and Astronomy, Aarhus University, DK-8000 Aarhus C, Denmark^b Instituto de Estructura de la Materia, IEM-CSIC, Serrano 123, E-28042 Madrid, Spain

ARTICLE INFO

Article history:

Received 28 August 2017

Received in revised form 24 March 2018

Accepted 1 May 2018

Available online 4 May 2018

Editor: W. Haxton

Keywords:

rp-Process

Capture rate

Electric dissociation

Three-body

Mean-field

ABSTRACT

We investigate the two-proton capture reaction of the prominent rapid proton capture waiting point nucleus, ^{68}Se , that produces the borromean nucleus ^{70}Kr ($^{68}\text{Se} + p + p$). We apply a recently formulated general model where the core nucleus, ^{68}Se , is treated in the mean-field approximation and the three-body problem of the two valence protons and the core is solved exactly. We compare using two popular Skyrme interactions, SLy4 and SkM*. We calculate $E2$ electromagnetic two-proton dissociation and capture cross sections, and derive the temperature dependent capture rates. We vary the unknown 2^+ resonance energy without changing any of the structures computed self-consistently for both core and valence particles. We find rates increasing quickly with temperature below 2–4 GK after which we find rates varying by about a factor of two independent of 2^+ resonance energy. The capture mechanism is sequential through the $f_{5/2}$ proton-core resonance, but the continuum background contributes significantly.

© 2018 The Authors. Published by Elsevier B.V. This is an open access article under the CC BY license (<http://creativecommons.org/licenses/by/4.0/>). Funded by SCOAP³.

1. Introduction

The abundance of most stable nuclei above iron in the universe can be understood as produced by various types of neutron capture [1,2]. However, production of about 40 stable isotopes cannot be explained in this way, but only through similar proton capture processes [3–7]. The basic ignition fuel is a large proton flux arising from a stellar explosion. The sequence of these reactions are then one proton capture after another until the proton dripline is reached and further captured protons are immediately emitted. This dripline nucleus usually must wait to beta-decay to a more stable nucleus which in turn can capture protons anew. This is the “rp-process” [8,9]. These p-nuclei are also believed to be produced by other methods: gamma-proton [4,10] and neutrino-proton processes [11,12].

The beta-decay waiting time is large for some of these nuclei along the dripline, which for that reason are denoted waiting points [13]. However, another path is possible to follow for borromean proton dripline nuclei where two protons, in contrast to

one, are necessary to produce a bound nucleus. Then two protons can be captured before beta-decay occurs [14,15]. The capture time and the corresponding mechanism are therefore important for the description of the outcome of these astrophysical processes [16,17].

We focus in this letter on one of these two-proton capture reactions leading from a prominent waiting point nucleus, ^{68}Se [18,19], to formation of the borromean proton dripline nucleus, ^{70}Kr ($^{68}\text{Se} + p + p$). Neither experimental nor theoretical specific reaction information are available at the moment [20–22].

Traditionally, the reactions have been described as sequential one-proton capture by tunneling through the combined Coulomb plus centrifugal barrier. The tunneling capture mechanisms have been discussed as direct, sequential and virtual sequential decay [23–26]. They are all accounted for in the present formulation. The capture rate depends on temperature through the assumed Maxwell–Boltzmann energy distribution. It is then important to know the energy dependence of the capture cross section for given resonance energies, and especially in the Gamow window [27].

Clearly the desired detailed description requires a three-body model which is available and even applied to the present processes [28,29]. However, the crucial proton-core potentials have so-far been chosen phenomenologically to produce the essentially un-

* Corresponding author.

E-mail address: dennish@phys.au.dk (D. Hove).

known, but crucial, single-particle energies. A new model involving both core and valence degrees of freedom was recently constructed to provide mean-field proton potentials derived from the effective nucleon–nucleon mean-field interaction [30–32]. In turn these potentials produce new and different effective three-body potentials, which in the present letter is exploited to investigate the two-proton capture rates.

The techniques are in place all the way from the solution of the coupled core and valence proton system [28,31,32], over the self-consistent three-body input and subsequent calculations [33, 34], to the capture cross sections and rates [35–38]. We shall first sketch the steps in the procedure used in the calculations. Then we shall discuss in more details the numerical results of interest for the astrophysical network computations, which calculates the abundances of the isotopes in the Universe.

2. Theoretical description

The basic formulation and the procedure are described in [28, 35,39]. The framework is the three-body technique but based on the proton-core potential derived through the self-consistently solved coupled core-plus-valence-protons equations [30,31]. The procedure is first to select the three-body method, second to formulate how to calculate the capture rate, and finally to choose the numerical parameters to be used in the computations.

2.1. Three-body method

The many-body problem is solved for a mean-field treated core interacting with two surrounding valence protons forming a three-body structure [28]. The details of this recent model are very elaborate, but already applied on two different neutron dripline nuclei [28,30]. It then suffices to sketch the method. The wave function is an antisymmetric product of a mean-field core Slater determinant and a three-body cluster wave function. The novel procedure is first to find the mean-field solution for the core-nucleons in the presence of the external field from the two valence protons. Second, the valence-proton to core interaction is obtained by folding the calculated mean-field core structure and the same mean-field nucleon–nucleon interaction. This provides the crucial interaction between each of the two valence protons and the core nucleus. The solution to this three-body problem redefines the external field acting on the core nucleons, and the procedure is repeated until convergence is reached.

The present application only relies on the three-body solution, where the self-consistently derived proton-core interaction is the main ingredient. We solve the three-body problem by use of the adiabatic expansion of the Faddeev equations [29] in hyperspherical coordinates. The key coordinate is the hyperradius, ρ , defined as the mean radial coordinate in the three-body system [39,41], that is

$$(2m_n + m_c)\rho^2 = m_n(\mathbf{r}_{v_1} - \mathbf{r}_{v_2})^2 + m_c \sum_{i=1}^2 (\mathbf{r}_{v_i} - \mathbf{R}_c)^2 \quad (1)$$

where m_n , m_c , \mathbf{r}_{v_1} , \mathbf{r}_{v_2} and \mathbf{R}_c are neutron mass, core mass, valence-proton and core center-of-mass coordinates, respectively. The hyperradius is supplemented by five hyperangles, and the three-body wave functions, Ψ_J , are found for given angular momenta, J , as described in [33]. When necessary the continuum is discretized by a large box confinement and the discretized continuum states, $\psi_j^{(i)}$, are calculated [35].

2.2. Reactions

The two-proton capture reaction $p + p + c \leftrightarrow A + \gamma$, where cross section, σ_{ppc} , and the photodissociation cross section, σ_γ^λ , of order λ are related [39]. The three-body energy, E , and the ground state energy, E_{gr} , determine the photon energy, $E_\gamma = E + |E_{gr}|$. The dissociation cross section is then given by

$$\sigma_\gamma^\lambda(E_\gamma) = \frac{(2\pi)^3(\lambda+1)}{\lambda((2\lambda+1)!!)^2} \left(\frac{E_\gamma}{\hbar c}\right)^{2\lambda-1} \frac{d}{dE} \mathcal{B}(E\lambda, 0 \rightarrow \lambda), \quad (2)$$

where the strength function for the $E\lambda$ transition,

$$\frac{d}{dE} \mathcal{B}(E\lambda, 0 \rightarrow \lambda) = \sum_i \left| \langle \psi_\lambda^{(i)} | \hat{\Theta}_\lambda | \Psi_0 \rangle \right|^2 \delta(E - E_i), \quad (3)$$

is given by the reduced matrix elements, $\langle \psi_\lambda^{(i)} | \hat{\Theta}_\lambda | \Psi_0 \rangle$, where $\hat{\Theta}_\lambda$ is the electric multipole operator, $\psi_\lambda^{(i)}$ is the wave function of energy, E_i , for all bound and (discretized) three-body continuum states in the summation. The capture reaction rate, R_{ppc} , is given by Ref. [37]

$$R_{ppc}(E) = \frac{8\pi}{(\mu_{cp}\mu_{cp,p})^{3/2}} \frac{\hbar^3}{c^2} \left(\frac{E_\gamma}{E}\right)^2 \sigma_\gamma^\lambda(E_\gamma), \quad (4)$$

where μ_{cp} and $\mu_{cp,p}$ are reduced masses of proton and core and proton-plus-core and proton, respectively. For the astrophysical processes in a gas of temperature, T , we have to average the rate in Eq. (4) over the corresponding Maxwell–Boltzmann distribution, $B(E, T) = \frac{1}{2} E^2 \exp(-E/T)/T^3$,

$$\langle R_{ppc}(E) \rangle = \frac{1}{2T^3} \int E^2 R_{ppc}(E) \exp(-E/T) dE, \quad (5)$$

where the temperature is in units of energy.

2.3. Interactions

The decisive interaction is related to the mean-field calculation of the core. We use the Skyrme interactions, SLy4 [42] and SkM* [43], both with acceptable global average properties. The application on one specific nucleus requires adjustment to provide the known borromean character, that is unbound proton-core $f_{5/2}$ resonance at 0.6 MeV [44] and two protons bound to the core. We achieve this by shifting all energies while leaving the established structure almost unaltered. The simplest consistent such modification is by scaling all the Skyrme strength parameters, t_i , by the same factors, 0.9515 and 0.98, respectively.

The density dependent t_3 -term of the Skyrme interaction can be viewed as a parametrized three-body potential. To simulate that effect we employ a short-range Gaussian, $S_0 \exp(-\rho^2/b^2)$, which depends on the hyperradius, ρ . This diagonal structure-less three-body Gaussian potential leaves the structure unaltered although the energies may change substantially. We choose $b = 6$ fm and $S_0 = -17.5$ MeV and $S_0 = -11.4$ MeV to reproduce the predicted 0^+ energy of -1.34 MeV [45,46] with the SLy4 and SkM* interactions, respectively. The unknown 2^+ energy is varied from almost bound (zero energy) to the top of the barrier by changing S_0 from -35.05 MeV (-37.8 MeV) to -26.22 MeV (-28.6 MeV) for the SLy4 (SkM*) interaction. This fine-tuning is necessary since the keV-scale of binding is crucial for tunneling through single MeV height barriers. The level of keV and even MeV-accuracy is beyond the capability of many-body model calculations.

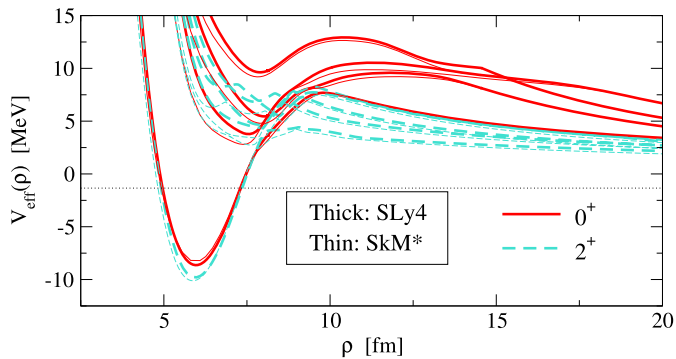


Fig. 1. The adiabatic potentials for the 0^+ (red, solid), and the 2^+ (light-blue, dashed) configuration in $^{68}\text{Se} + p + p$ using the SLy4 (thick) and SkM* (thin) Skyrme interaction between core and valence protons, scaled to reproduce the experimental $f_{5/2}$ resonance energy of 0.6 MeV in $^{68}\text{Se} + p$ [44]. The dotted horizontal line is the 0^+ energy at -1.34 MeV. The gaussian three-body potential is not included. (For interpretation of the colors in the figure(s), the reader is referred to the web version of this article.)

3. Effective three-body potentials

The elaborate numerical calculations for SLy4 and SkM* produce the sets of coupled “one-body” potentials depending on hyperradius as shown in Fig. 1 for both 0^+ (solid) and 2^+ (dashed) states. The thick and thin curves are, respectively, the potentials obtained with the SLy4 and SkM* interactions, which, as seen in the figure, are very similar to each other. The continuations beyond the 20 fm in the figure are almost quantitatively Coulomb plus centrifugal behavior and as such reveal no surprises. The kinks and fast bends reflect avoided crossings and related structure changes. They are especially abundant at small distances and around the barriers.

The 0^+ ground-state at -1.34 MeV [45,46] has structure corresponding to the configuration of the pronounced minimum in the lowest 0^+ potential. This is the final state in the capture process independent of the specific mechanism. No 0^+ resonances (above zero energy) are produced by the potentials in Fig. 1.

The decisive capture process proceeds within the 2^+ continuum from the large to the short-distance attractive region of the potentials shown in Fig. 1. The lowest minimum is rather similar to the 0^+ minimum but the non-adiabatic repulsive terms, omitted in the figure, increase the energy substantially. Unfortunately nothing is known about a 2^+ resonance which would strongly influence the capture rate. Consequently the strength, S_0 , is used to vary the position of the 2^+ resonance from almost bound to disappearance above the barriers. Both the resonance energy, the height, and the rather broad Coulomb shape of the barrier strongly influence the capture process.

The structure of these potentials is substantially simpler than those obtained in [28] where low-lying single-proton states $p_{3/2}$ and $f_{5/2}$ both appeared. This simplification results from using the nucleon–nucleon mean-field effective interaction to calculate the proton-core potential. It is a novel deduction embedded in the design of our model, arising naturally due to identical interactions for both core and valence particles. There is no single-particle states of the other parity implying that no 1^- three-body resonance state appear in the low-energy region for neither of these Skyrme interactions.

4. Quantitative results

The all-important core-valence proton potential is derived naturally and unambiguously by our mean-field core treatment. As a result the two-proton capture cross section follows directly, only depending on the three-body resonance level. This is discussed in

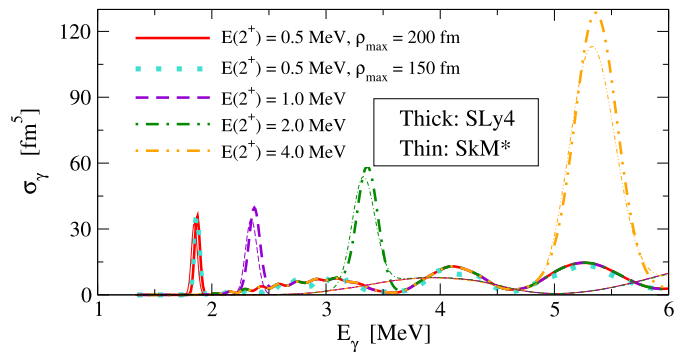


Fig. 2. The electromagnetic $E2$ dissociation cross section, $\sigma_\gamma^{(\lambda=2)}(E_\gamma)$, for the process, $^{70}\text{Kr} + \gamma \rightarrow ^{68}\text{Se} + p + p$, as a function of photon energy for the SLy4 (thick) and SkM* (thin) interactions. The 0^+ final state energy is -1.34 MeV and the 2^+ resonance energies are $E = 0.5, 1.0, 2.0,$ and 4.0 MeV, respectively. The discretized continuum states are with box sizes of $\rho_{\text{max}} = 150, 200$ fm.

the following section, after which the resulting temperature averaged reaction rates are presented. This is supplemented by a discussion of the reaction mechanism and its implication for the possible reactions.

4.1. Cross section

The incident flux of low-energy protons on the core nucleus may result in capture. The corresponding cross section is most easily obtained from calculation of the inverse reaction, that is photodissociation of the 0^+ ground state, Ψ_0 , of ^{70}Kr . The discretized continuum states, $\psi_\lambda^{(i)}$, are computed and the cross section is obtained from Eqs. (3) and (2) with $\lambda = 2$. The photodissociation cross section, obtained from Eq. (2), is shown in Fig. 2 as function of the three-body energy.

The peaks in the capture cross section occur at experimentally unknown resonance energies where the tunneling probability is large. We therefore vary the energy from 0.5 MeV to 4.0 MeV where the widths of the peaks in the cross section increase with energy as the top of the barrier is approached. The crucial quantity is the resonance energy as tested within the present framework by including less adiabatic potentials than needed for convergence. By readjusting to the same resonance energy by use of the three-body potential we recover the cross section in Fig. 2.

These features are simply understood as enhanced spatial overlaps between the 2^+ continuum states in the resonance region and the ground state wave function, expressed through Eq. (3). Beside the resonance contributions we also find significant, although several orders of magnitude smaller, background contributions, which is independent of a sufficiently large discretization box [40].

4.2. Capture rates

The capture cross sections are the main ingredient in the calculation of the two-proton absorption rate appropriate for the temperature dependent astrophysical network computation. The average rate in Eq. (5) is shown in Fig. 3 as a function of temperature. The left and right panels correspond to the results obtained with the SLy4 and SkM* interactions, respectively. The Boltzmann smearing factor produces very smooth and qualitative similar curves. They are zero at zero temperature and energy, because the barrier is infinitely thick. All rates then increase to a maximum at the Gamow peak where the best compromise is reached between the decreasing temperature distribution and the increasing tunneling probability. The main difference between the SLy4 and SkM* results arises from the smaller background contribution in the second case. This fact produces smaller rates at

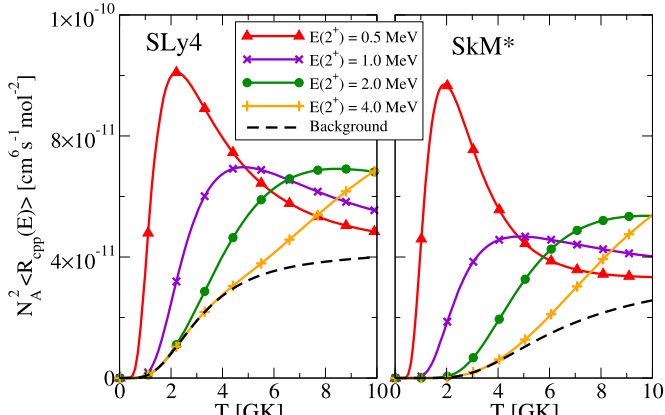


Fig. 3. Reaction rates, using SLy4 (left) and SkM* (right) interactions, for the radiative capture process $^{68}\text{Se} + p + p \rightarrow ^{70}\text{Kr} + \gamma$, as function of temperature for the different 2^+ resonance energies in Fig. 2. The black dashed curves are background contributions.

high temperatures, although the general features are very much the same in both cases.

The peak contribution moves to higher energy and becomes smoother with increasing resonance energy. Above temperatures of a few GK the average rate variation is moderate and the size roughly of order $\simeq 6 \times 10^{-11} \text{ cm}^6 [N_A \text{ mol}]^{-2} \text{ s}^{-1}$ or $\simeq 4 \times 10^{-11} \text{ cm}^6 [N_A \text{ mol}]^{-2} \text{ s}^{-1}$, depending on the Skyrme interaction. A low-lying resonance energy corresponds to low-lying peak position of larger height. We emphasize that the background without resonance contribution obviously is smaller but sizable as soon as the temperature exceeds about 4 GK ($\sim 0.34 \text{ MeV}$). In other words, if temperatures are in the astrophysically interesting range below about 1 GK, the size variations are substantial, and vice versa above a few GK the details from the microscopic origin are smeared out.

The actual size of the rate may reveal deceivingly little variation at the relatively high temperatures. However, the barrier height and width are all-decisive and both may easily be different for other systems where the single-particle structure at the Fermi energy is different and perhaps more complicated as studied in [28]. The relatively large 2^+ background contribution might suggest corresponding relative large 0^+ continuum contributions. However, the 0^+ barriers in Fig. 1 are larger and the $0^+ \rightarrow 0^+$ transition as well require processes involving atomic electrons. It is again worth emphasizing that a superficially more complete calculation with many coupled potentials would provide the same rates after adjusting to the same resonance energy.

4.3. Reaction mechanism

The rate depends on the capture mechanism. We are here only concerned with three-body capture, but a dense environment would enhance four-body capture processes as discussed in [36]. The overall three-body process is tunneling through a barrier of particles in a temperature distribution of given density. Once inside the relatively thick barrier they have essentially only the option of emitting photons to reach the bound ground-state. However, the first of this two-step process can occur through different mechanisms, where the most obvious possibility is to be captured in different angular momentum states. The conservation of angular momentum and parity quantum numbers are crucial in connection with resonance positions.

If low-lying 1^- continuum states are allowed they would be preferred. If 1^- states are prohibited 2^+ continuum states would be preferred, and the system would have a longer effective lifetime.

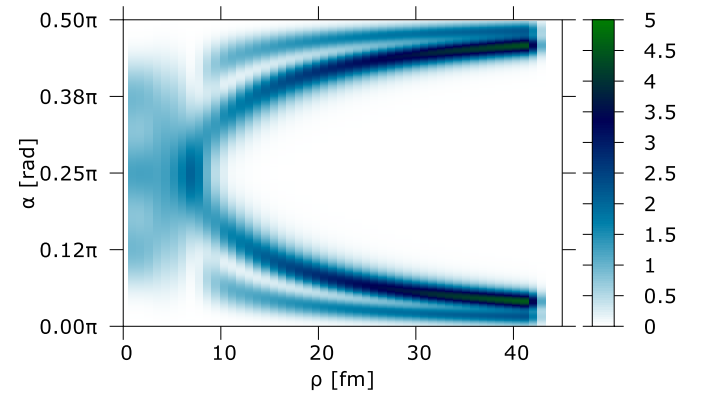


Fig. 4. The probability of the three-body, $^{68}\text{Se} + p + p$, wave function for the lowest allowed potential with the SLy4 interaction, integrated over directional angles ($\sin^2(\alpha) \cos^2(\alpha) \int |\Phi_n(\alpha, \rho, \Omega_x, \Omega_y)|^2 d\Omega_x d\Omega_y$), as a function of hyperradius, ρ , and hyperangle, α , related to the Jacobi coordinate system where “x” is between core and proton.

This could very well be why some systems appear to be critical waiting point nuclei. In general, low-lying resonances enhance the contributions substantially. This selection depends strongly on the nucleus under investigation.

For a given angular momentum of the three-body continuum states, we still may encounter several qualitatively different ways of absorbing two protons from the continuum [47]. These mechanisms were discussed in [23] for the inverse process of disassociation, that is direct, sequential and virtual sequential decay. They are all accounted for in the present formulation. In [28] we concluded that the direct process is most probable for very low three-body energy when two-body subsystems are unbound. If the energy is larger than stable two-body substructures such intermediate vehicles enhance the rates and the mechanism is sequential.

Even when it is energetically forbidden to populate two-body resonance states it may be advantageous to exploit these structures virtually while tunneling through an also energetically forbidden barrier. This is appropriately named the virtual sequential two-body mechanism. It may be appropriate to emphasize that a similar three-body virtual mechanism is forbidden because the three-body energy is conserved in contrast to the energy of any two-body subsystem.

The mechanism for the present capture process is revealed in Fig. 4 where the 2^+ probability integrated over the directional angles is shown for the lowest potential as function of hyperradius and one of the Jacobi angles. It is a strikingly simple structure for hyperradii larger than about 15 fm, which for these coordinates is equivalent to one proton at that distance from the center of mass of the combined proton-core system. Since the Jacobi angle, α , is either close to zero or $\pi/2$, this simply means that one proton is staying very close to the core for all these hyperradii. Eventually also this proton has to move away from the core, since no bound state exists. But this process is sequential through the substructure characterized as the proton-core $f_{5/2}$ resonance.

The higher-lying configurations corresponding to the three following potentials also show precisely the same $f_{5/2}$ structure. This is explained by combining the compact proton-core $f_{5/2}$ resonance with one non-interacting (apart from Coulomb and centrifugal) distant proton in any angular momentum configuration consistent with a 2^+ structure. The angular momenta capable of combining with $f_{5/2}$ to produce 2^+ are $p_{1/2}$, $p_{3/2}$, $f_{5/2}$, $f_{7/2}$, and $h_{9/2}$. This also implies that for temperatures much smaller than the $f_{5/2}$ resonance energy it would be energetically advantageous to start the capture process in a configuration corresponding to direct three-body capture. The change of structure, around avoided

level crossings, to two-body resonance configurations would then greatly reduce the barrier and substantially enhance the capture rate.

5. Conclusion

The new model that treats the core and the two valence particles self-consistently and simultaneously is applied on the waiting point nucleus (^{68}Se) for the astrophysical rp-process. This is done with only two phenomenological tuning parameters, that is scaling of the nucleon–nucleon interaction strength and addition of structureless three-body potential. Both adjustments leave the structure unchanged while shifting the energies to desired positions. The results are therefore much less arbitrary than usual three-body calculations, as demonstrated by the robustness against changes of the Skyrme interactions, SLy4 and SkM*. Adding two protons, but not one, produces a bound system, ^{70}Kr , which is then a borromean nucleus.

We calculate the radiative two-proton capture rate as function of temperature for different resonance energies. We investigate the mechanism and find that sequential capture of one proton after the other by far is dominating. The first available single-particle resonance state, $f_{5/2}$, is the vehicle, whereas the other proton can approach in continuum states of even higher angular momentum. After tunneling through the barrier into the 2^+ resonance state, in practice only E2 electric transition to the ground state is allowed. Background capture through non-resonance continuum states also contributes significantly to the capture process. The sequential 2^+ capture mechanism might for other nuclei be replaced by for example the normally larger 1^- capture.

We emphasize that the crucial properties are the energies and angular momentum quantum numbers of the single-particle core states at the Fermi surface. The cross sections and capture rates can therefore be substantially different for another nucleus. We have the crucial properties determined by the procedure, which moves the uncertainties from the three-body level to the choices made in the many-body treatment. Different Skyrme interactions suitable for dripline nuclei give similar results for the same nucleus, whereas inappropriate Skyrme interactions might give very different results. The point is that we need more information to choose wisely, but nucleon–nucleon effective interactions can now be used directly to predict electromagnetic capture rates. Even more generally, this line of deduction can also be used if the mean-field treatment is replaced altogether by something better.

In conclusion, the two-proton capture rates at a waiting point at the dripline are successfully calculated with a conceptually relatively simple, but technically advanced, new model. The same effective nucleon–nucleon interaction is used for both the nuclear mean-field and the proton-core calculations. The temperature dependent rate and the corresponding capture mechanism are calculated with less ambiguity than in previous calculations. A number of applications are now feasible.

Acknowledgements

This work was funded by the Danish Council for Independent Research DFF Natural Science and the DFF Sapere Aude program. This work has been partially supported by the Spanish Ministerio de Economía y Competitividad under Project FIS2014-51971-P.

References

- [1] G.J. Mathews, R.A. Ward, *Rep. Prog. Phys.* **48** (1985) 1371.
- [2] A. Barlett, et al., *Phys. Rev. C* **74** (2006) 015802.
- [3] E.M. Burbidge, et al., *Rev. Mod. Phys.* **29** (1957) 547.
- [4] M. Arnould, S. Goriely, *Phys. Rep.* **384** (2003) 1–84.
- [5] T. Rauscher, N. Dauphas, I. Dillmann, C. Fröhlich, Z. Fülöp, G. Gyürky, *Rep. Prog. Phys.* **76** (2013) 066201.
- [6] R. Reifarh, C. Lederer, Fäppeler, *J. Phys. G, Nucl. Part. Phys.* **41** (2014) 053101.
- [7] H. Palme, K. Lodders, A. Jones, in: A.M. Davis (Ed.), *Solar System Abundances of the Elements in Planets, Asteroids, Comets and the Solar System*, 2014, pp. 15–36.
- [8] H. Schatz, et al., *Phys. Rep.* **294** (1998) 167.
- [9] B.A. Brown, R.R.C. Clement, H. Schatz, A. Volya, *Phys. Rev. C* **65** (2002) 045802.
- [10] S.E. Woosley, W.M. Howard, *Astrophys. J. Suppl.* **36** (1978) 285.
- [11] C. Fröhlich, G. Martínez-Pinedo, M. Liebendörfer, F.-K. Thielemann, E. Bravo, W.R. Hix, K. Langanke, N.T. Zinner, *Phys. Rev. Lett.* **96** (2006) 142502.
- [12] C. Fröhlich, P. Hauser, M. Liebendörfer, G. Martínez-Pinedo, et al., *Astrophys. J.* **637** (2006) 415.
- [13] M. Oinen, et al., *Phys. Rev. C* **61** (2000) 035801.
- [14] L.V. Grigorenko, M.V. Zhukov, *Phys. Rev. C* **72** (2005) 015803.
- [15] L.V. Grigorenko, R.C. Johnson, I.G. Mukha, I.J. Thompson, M.V. Zhukov, *Phys. Rev. C* **64** (2001) 054002.
- [16] J. Görres, M. Wiescher, F.-K. Thielemann, *Phys. Rev. C* **51** (1995) 392.
- [17] H. Schatz, *Int. J. Mass Spectrom.* **251** (2006) 293.
- [18] P. Schury, et al., *Phys. Rev. C* **75** (2007) 055801.
- [19] X.L. Tu, et al., *Phys. Rev. Lett.* **106** (2011) 112501.
- [20] M. Thoennessen, *Rep. Prog. Phys.* **67** (2004) 1187.
- [21] J. Erler, et al., *Nature* **486** (2012) 509.
- [22] M. Pfützner, M. Karny, L.V. Grigorenko, K. Riisager, *Rev. Mod. Phys.* **84** (2012) 567.
- [23] A.S. Jensen, D.V. Fedorov, E. Garrido, *J. Phys. G, Nucl. Part. Phys.* **37** (2010) 064027.
- [24] E. Garrido, D.V. Fedorov, A.S. Jensen, H.O.U. Fynbo, *Nucl. Phys. A* **748** (2005) 27.
- [25] S. Chekanov, et al., *Eur. Phys. J. C* **51** (2007) 289.
- [26] R. Álvarez-Rodríguez, H.O.U. Fynbo, A.S. Jensen, E. Garrido, *Phys. Rev. Lett.* **100** (2008) 192501.
- [27] C. Iliadis, *Nuclear Physics of Stars*, John Wiley & Sons, 2015.
- [28] D. Hove, A.S. Jensen, H.O.U. Fynbo, N.T. Zinner, D.V. Fedorov, E. Garrido, *Phys. Rev. C* **93** (2016) 024601.
- [29] E. Garrido, D.V. Fedorov, A.S. Jensen, *Phys. Rev. C* **69** (2004) 024002.
- [30] D. Hove, E. Garrido, P. Sarriguren, D.V. Fedorov, H.O.U. Fynbo, A.S. Jensen, N.T. Zinner, *Phys. Rev. C* **95** (2017) 061301(R).
- [31] D. Hove, E. Garrido, P. Sarriguren, D.V. Fedorov, H.O.U. Fynbo, A.S. Jensen, N.T. Zinner, arXiv:1705.08718, 2017.
- [32] D. Hove, E. Garrido, A.S. Jensen, P. Sarriguren, H.O.U. Fynbo, D.V. Fedorov, N.T. Zinner, *Few-Body Syst.* **58** (2017) 33.
- [33] E. Nielsen, D.V. Fedorov, A.S. Jensen, E. Garrido, *Phys. Rep.* **347** (2001) 373.
- [34] A.S. Jensen, K. Riisager, D.V. Fedorov, E. Garrido, *Rev. Mod. Phys.* **76** (2004) 215.
- [35] E. Garrido, *Few-Body Syst.* **56** (2015) 829.
- [36] R. de Diego, D.V. Fedorov, E. Garrido, A.S. Jensen, *J. Phys. G, Nucl. Part. Phys.* **37** (2010) 115105.
- [37] R. de Diego, et al., *Phys. Lett. B* **695** (2011) 324.
- [38] R. de Diego, E. Garrido, D.V. Fedorov, A.S. Jensen, *Europhys. Lett.* **90** (2010) 52001.
- [39] E. Garrido, A.S. Jensen, D.V. Fedorov, *Phys. Rev. C* **91** (2015) 054003.
- [40] E. Garrido, *Few-Body Syst.* **56** (2015) 829.
- [41] D. Hove, et al., *Phys. Rev. C* **90** (2014) 064311.
- [42] E. Chabanat, P. Bonche, P. Haensel, J. Meyer, R. Schaeffer, *Nucl. Phys. A* **635** (1998) 231.
- [43] J. Bartel, Ph. Quentin, M. Brack, C. Guet, H.-B. Håkansson, *Nucl. Phys. A* **386** (1982) 79.
- [44] M.D. Santo, et al., *Phys. Lett. B* **738** (2014) 453.
- [45] M. Wang, G. Audi, A.H. Wapstra, F.G. Kondev, M. MacCormick, X. Xu, B. Pfeiffer, *Chin. Phys. C* **36** (2012) 1603.
- [46] G. Audi, et al., *Chin. Phys. C* **36** (2012) 1287.
- [47] E. Garrido, R. de Diego, D.V. Fedorov, A.S. Jensen, *Eur. Phys. J. A* **47** (2011) 102.